Research Square

Preprints are preliminary reports that have not undergone peer review.
They should not be considered conclusive, used to inform clinical practice,
or referenced by the media as validated information.

Photonic Generation of Wideband Linear Frequency-Modulated Radar Waveforms with High Spurious Suppression for Spaceborne Tracking

SATHISHA R N

sathisharyan@sit.ac.in

Siddaganga Institute of Technology https://orcid.org/0000-0001-8031-7611

Research Article

Keywords: microwave photonics, radar transmitter, frequency quadrupling, dual-parallel Mach-Zehnder modulator, linear frequency modulation, range resolution, pulse compression, phase noise decorrelation, optical heterodyning

Posted Date: November 12th, 2026

DOI: https://doi.org/10.21203/rs.3.rs-11706743/v1

License: This work is licensed under a Creative Commons Attribution 4.0 International License.
Read Full License

Additional Declarations: The authors declare no competing interests.

Photonic Generation of Wideband Linear Frequency-Modulated Radar Waveforms With High Spurious Suppression for Space Tracking

Sathisha R. N.
Department of Electronics and Telecommunication Engineering
Siddaganga Institute of Technology, Tumakuru 572103, Karnataka, India
Email: satisharyan@gmail.com ORCID: 0000-0001-8031-7611

November 2026

Abstract

High-resolution spaceborne imaging and ground tracking radars operating in the X-band require multi-gigahertz chirp bandwidths with low phase noise and high radio-frequency spurious suppression. Conventional electronic up-conversion chains suffer from high phase noise multiplication and limited instantaneous bandwidth. In this paper, we investigate the photonic generation of wideband linear frequency-modulated (LFM) radar signals building upon microwave photonic transmitter architectures. We present a dual-parallel Mach-Zehnder modulator (DPMZM) frequency quadrupling architecture that up-converts a low-frequency 2.4 GHz electronic local oscillator (LO) and a 500 MHz baseband chirp to a clean 9.6 GHz X-band carrier with 2.0 GHz instantaneous chirp bandwidth. By biasing the sub-modulators at the minimum transmission point (MITP) and driving them via a 90° RF hybrid coupler, the optical carrier and odd-order optical sidebands are canceled, achieving a radio-frequency spurious suppression ratio (RFSSR) exceeding 57 dB, compared with less than 10 dB for a conventional single-drive MZM. We provide a comprehensive tolerance analysis examining RF hybrid phase/amplitude imbalances and DC bias voltage drift. Furthermore, we mathematically analyze the phase coherence of optical heterodyning between two free-running lasers versus single-laser external modulation. We prove that free-running optical heterodyning experiences laser linewidth phase diffusion where phase variance $\sigma_\phi^2 = 2\pi\Delta\nu\tau_{\text{echo}}$ exceeds 2.5 rad for a 100 kHz linewidth over a 10 μs echo delay (1.5 km target range), causing decorrelation and severe pulse compression degradation. Conversely, single-laser photonic modulation provides common-mode phase cancellation, preserving pulse compression matched-filter gains. The generated 2.0 GHz photonic chirp delivers a fourfold improvement in range resolution (from 30 cm to 7.5 cm), resolving adjacent radar scatterers spaced 0.6 m apart with Taylor-windowed peak-to-sidelobe ratios exceeding 30 dB.

Keywords: Microwave photonics, radar transmitter, frequency quadrupling, dual-parallel Mach-Zehnder modulator (DPMZM), linear frequency modulation (LFM), phase noise, pulse compression, range resolution, tolerance analysis.

1 Introduction

Modern spaceborne synthetic aperture radar (SAR), planetary tracking, and telemetry networks demand radar transmitters capable of synthesizing multi-gigahertz instantaneous bandwidths at high carrier frequencies with exceptional spectral purity [1, 2]. The Indian

Preprint submitted to IEEE for possible publication. Copyright may be transferred without notice.

Space Research Organisation (ISRO), through tracking telemetry and command networks (ISTRAC), has specifically emphasized photonic radar transmitter architectures capable of generating stable, low-phase-noise microwave signals at X-band and beyond [3].

Conventional microwave transmitters generate high-frequency linear frequency-modulated (LFM) chirps through cascading electronic frequency multipliers, analog mixers, and band-pass filters. However, electronic up-conversion chains face physical bottlenecks:

1. Frequency multiplication degrades phase noise by $20\log_{10}(N)$ dB, where N is the multiplication factor [4].
2. Mixer non-linearities introduce in-band intermodulation spurs and harmonics that demand complex, bulky analog filtering networks [1].
3. High-speed digital-to-analog converters (DACs) capable of synthesizing multi-gigahertz chirps directly at X-band consume substantial DC power and suffer from limited effective number of bits (ENOB) [4].

Microwave photonics (MWP) overcomes these electronic barriers by leveraging the wide bandwidth, low transmission loss, and electromagnetic interference (EMI) immunity of optical components [2, 1]. Two optical generation schemes have been proposed in the literature: optical heterodyning of two independent laser diodes [6], and external electro-optic modulation driven by a stable, low-frequency microwave reference [4, 5].

While dual-laser optical heterodyning offers wide continuous frequency tunability by adjusting laser emission wavelengths, free-running semiconductor lasers exhibit uncorrelated phase drift that degrades the coherence of radar echoes over target round-trip delays [6]. Conversely, external modulation using integrated lithium niobate ($LiNbO_3$) or silicon photonic dual-parallel Mach-Zehnder modulators (DPMZM) uses a single optical carrier, ensuring common-mode phase cancellation and phase noise performance linked to the low-frequency RF seed oscillator [4, 1].

In this paper, we address the design and phase-coherence limits of photonic radar transmitters for spaceborne and tracking applications. The paper is organized as follows:

- Section II derives the mathematical formulation of DPMZM-based frequency quadrupling, optical sideband suppression, and wideband photonic chirp synthesis.
- Section III formulates the phase diffusion of radar echoes, proving why free-running two-laser heterodyning fails pulse-compression matched filtering over orbital distances, whereas single-laser DPMZM architectures preserve full coherence.
- Section IV evaluates numerical simulation results, demonstrating over 57 dB RF spurious suppression, tolerance sensitivity, and fourfold range resolution enhancement (7.5 cm resolution).
- Section V reviews implementation constraints, including DC bias drift control and photodetector power handling for space platforms.
- Section VI concludes the paper.

2 System Architecture and Mathematical Model

The overall architecture of the photonic radar transmitter is illustrated in Fig. 1. A continuous-wave (CW) single-mode distributed feedback (DFB) laser provides an optical carrier at angular frequency $\omega_c = 2\pi c/\lambda$ with optical power P_0. The optical field entering the modulator is:

$$E_{\text{in}}(t) = \sqrt{P_0}\,\exp\left(j\left[\omega_c t + \phi_0(t)\right]\right), \tag{1}$$

Preprint submitted to IEEE for possible publication. Copyright may be transferred without notice.

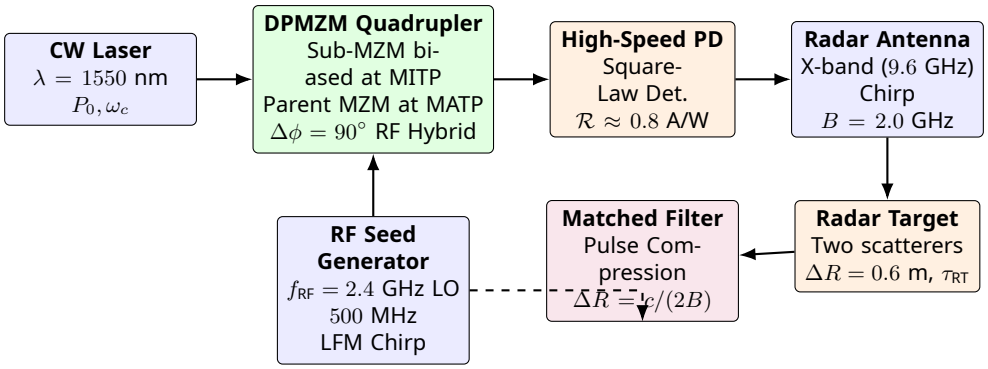


Figure 1: Photonic radar transmitter architecture based on a DPMZM frequency quadrupler, optical carrier suppression, and coherent radar pulse compression.

where $\phi_0(t)$ denotes laser phase noise characterized by a Lorentzian linewidth $\Delta\nu$.

2.1 DPMZM Frequency Quadrupling Formulation

The DPMZM integrates two parallel sub-modulators (MZM-A and MZM-B) nested inside a main parent Mach-Zehnder interferometer. An electronic reference generates an intermediate frequency LO signal at $f_{\mathrm{RF}} = 2.4$ GHz alongside a baseband LFM chirp. The drive signal is passed through a 90° electrical hybrid coupler:

$$V_{\mathrm{RF},A}(t) = V_m \cos(\omega_{\mathrm{RF}} t), \qquad V_{\mathrm{RF},B}(t) = V_m \sin(\omega_{\mathrm{RF}} t). \tag{2}$$

Defining the modulation index as $\beta = \pi V_m / V_\pi$, where V_π is the half-wave switching voltage, the optical fields leaving the two sub-MZMs are:

$$E_A(t) = \frac{E_{\mathrm{in}}(t)}{2}\left[\exp\left(j\left[\beta\cos(\omega_{\mathrm{RF}}t) + \frac{\theta_A}{2}\right]\right) + \exp\left(-j\left[\beta\cos(\omega_{\mathrm{RF}}t) + \frac{\theta_A}{2}\right]\right)\right], \tag{3}$$

$$E_B(t) = \frac{E_{\mathrm{in}}(t)}{2}\left[\exp\left(j\left[\beta\sin(\omega_{\mathrm{RF}}t) + \frac{\theta_B}{2}\right]\right) + \exp\left(-j\left[\beta\sin(\omega_{\mathrm{RF}}t) + \frac{\theta_B}{2}\right]\right)\right], \tag{4}$$

where θ_A and θ_B represent the DC bias phase shifts of the two sub-modulators. To achieve carrier suppression, both sub-modulators are biased at the minimum transmission point (MITP), setting $\theta_A = \theta_B = \pi$. Under MITP biasing, the Jacobi-Anger expansion yields:

$$E_A(t) = E_{\mathrm{in}}(t)\sum_{n=1}^{\infty} 2j^{2n-1} J_{2n-1}(\beta)\cos\left[(2n-1)\omega_{\mathrm{RF}}t\right]\sin\left(\frac{\pi}{2}\right) = 0 \quad (\text{for even orders}), \tag{5}$$

which eliminates all even-order optical sidebands (including the optical carrier at ω_c) from the sub-modulator outputs:

$$E_A(t) = -2E_{\mathrm{in}}(t)\left[J_1(\beta)\cos(\omega_{\mathrm{RF}}t) - J_3(\beta)\cos(3\omega_{\mathrm{RF}}t) + J_5(\beta)\cos(5\omega_{\mathrm{RF}}t) - \ldots\right], \tag{6}$$

$$E_B(t) = -2E_{\mathrm{in}}(t)\left[J_1(\beta)\sin(\omega_{\mathrm{RF}}t) + J_3(\beta)\sin(3\omega_{\mathrm{RF}}t) + J_5(\beta)\sin(5\omega_{\mathrm{RF}}t) + \ldots\right]. \tag{7}$$

The two optical paths are recombined in the parent interferometer with a static DC phase difference θ_P. When the parent modulator is biased at the maximum transmission point (MATP, $\theta_P = 0$ or π), constructive and destructive interference isolates specific harmonics. Combining the optical fields with an optical 90° phase shift ($\theta_P = \pi/2$) cancels the dominant first-order sidebands ($\pm 1\omega_{\mathrm{RF}}$), leaving the second-order sidebands ($\pm 2\omega_{\mathrm{RF}}$) as the dominant optical spectral components:

$$E_{\mathrm{out}}(t) = E_A(t) + E_B(t)e^{j\pi/2} \approx E_{\mathrm{in}}(t)\left[J_2(\beta)e^{j(\omega_c + 2\omega_{\mathrm{RF}})t} + J_2(\beta)e^{j(\omega_c - 2\omega_{\mathrm{RF}})t}\right]. \tag{8}$$

Preprint submitted to IEEE for possible publication. Copyright may be transferred without notice.

2.2 Photodetector Square-Law Beating

The output optical field illuminates a high-speed PIN photodiode with responsivity $\mathcal{R}$. The resulting photocurrent is:

$$\begin{aligned} i_{\mathsf{pd}}(t) &= \mathcal{R}\,|E_{\mathsf{out}}(t)|^2 \\ &= \mathcal{R}P_0 \left| J_2(\beta)e^{j(\omega_c+2\omega_{\mathsf{RF}})t} + J_2(\beta)e^{j(\omega_c-2\omega_{\mathsf{RF}})t} \right|^2 \\ &= 2\mathcal{R}P_0 J_2^2(\beta)\left[1+\cos(4\omega_{\mathsf{RF}}t)\right]. \end{aligned} \tag{9}$$

The optical carrier phase noise $\phi_0(t)$ cancels because both second-order sidebands originate from the same laser source:

$$[\omega_c t + 2\omega_{\mathsf{RF}}t + \phi_0(t)] - [\omega_c t - 2\omega_{\mathsf{RF}}t + \phi_0(t)] = 4\omega_{\mathsf{RF}}t. \tag{10}$$

Equation (9) produces an RF output frequency of:

$$f_{\mathsf{out}} = 4f_{\mathsf{RF}} = 4 \times 2.4\ \mathsf{GHz} = 9.6\ \mathsf{GHz}, \tag{11}$$

synthesizing an X-band microwave carrier directly from an S-band oscillator without analog frequency multipliers or mixer chains.

2.3 Modulator Imperfection and Tolerance Analysis

In practical space-qualified implementations, performance is limited by three physical non-idealities: DC bias voltage drift ($\Delta\theta_A, \Delta\theta_B$), RF hybrid phase imbalance ($\Delta\phi_{\mathsf{RF}}$), and RF amplitude mismatch ($\epsilon = V_{m,B}/V_{m,A} - 1$). In the presence of these errors, the optical output field becomes:

$$E_{\mathsf{out}}(t) = E_A(t, \Delta\theta_A) + (1+\epsilon)E_B(t, \Delta\theta_B, \Delta\phi_{\mathsf{RF}})e^{j(\pi/2+\Delta\theta_P)}. \tag{12}$$

Expanding this field reveals that DC bias offset $\Delta\theta$ leaks residual optical carrier power proportional to $\sin^2(\Delta\theta/2)J_0^2(\beta)$, while RF hybrid phase imbalance $\Delta\phi_{\mathsf{RF}}$ prevents complete cancellation of the first-order sidebands, leaking energy into fundamental (f_{RF}) and third-harmonic ($3f_{\mathsf{RF}}$) beat notes. The resulting spurious suppression ratio degrades according to:

$$\mathsf{RFSSR} \approx 10\log_{10}\left(\frac{J_2^4(\beta)}{J_1^2(\beta)J_3^2(\beta)\sin^2(\Delta\phi_{\mathsf{RF}}) + J_0^2(\beta)J_4^2(\beta)\sin^2(\Delta\theta_{\mathsf{bias}}) + 10^{-6}}\right). \tag{13}$$

2.4 Photonic LFM Chirp Scaling

When an electronic baseband linear frequency-modulated chirp is applied:

$$s_{\mathsf{chirp}}(t) = \cos\left(2\pi f_0 t + \pi K_r t^2\right), \quad 0 \le t \le T_p, \tag{14}$$

where f_0 is the start frequency, $K_r = B_{\mathsf{chirp}}/T_p$ is the chirp rate, B_{chirp} is the electronic bandwidth (500 MHz), and T_p is pulse duration ($2.0\ \mu$s), the quadrupling process scales both the instantaneous carrier and chirp bandwidth by a factor of 4:

$$i_{\mathsf{chirp}}(t) \propto \cos\left(2\pi(4f_0)t + \pi(4K_r)t^2\right). \tag{15}$$

The synthesized radar chirp exhibits an instantaneous bandwidth of:

$$B_{\mathsf{opt}} = 4 \times B_{\mathsf{chirp}} = 4 \times 500\ \mathsf{MHz} = 2.0\ \mathsf{GHz}. \tag{16}$$

The radar range resolution ΔR is governed by the speed of light c and chirp bandwidth:

$$\Delta R = \frac{c}{2B}. \tag{17}$$

For the electronic reference ($B = 500$ MHz), $\Delta R = 30.0$ cm. For the quadrupled photonic waveform ($B = 2.0$ GHz), range resolution improves to:

$$\Delta R_{\text{photonic}} = \frac{3 \times 10^8 \text{ m/s}}{2 \times 2.0 \times 10^9 \text{ Hz}} = 7.5 \text{ cm}. \tag{18}$$

3 Phase Noise and Echo Coherence Analysis

A key question in microwave photonics is whether optical heterodyning between two independent, wavelength-offset lasers can replace external modulator-based multiplication. Here we evaluate the matched-filter coherence over target round-trip delays.

3.1 Free-Running Two-Laser Heterodyning Decoherence

Consider generating a 9.6 GHz carrier by photodiode beating of two free-running lasers emitting at angular frequencies ω_1 and $\omega_2 = \omega_1 + \Omega_{\text{RF}}$:

$$E_1(t) = \sqrt{P_1}\exp\left(j\left[\omega_1 t + \phi_1(t)\right]\right), \qquad E_2(t) = \sqrt{P_2}\exp\left(j\left[\omega_2 t + \phi_2(t)\right]\right), \tag{19}$$

where $\phi_1(t)$ and $\phi_2(t)$ are uncorrelated Wiener phase noise processes with Lorentzian linewidths $\Delta\nu_1$ and $\Delta\nu_2$. The transmitted microwave current is:

$$i_{\text{tx}}(t) \propto \cos\left(\Omega_{\text{RF}} t + \Delta\phi_{\text{tx}}(t)\right), \quad \Delta\phi_{\text{tx}}(t) = \phi_2(t) - \phi_1(t). \tag{20}$$

The transmitted signal travels to a radar target at range R, reflecting with a round-trip delay $\tau_{\text{RT}} = 2R/c$. The received echo is:

$$i_{\text{rx}}(t) = \alpha_{\text{target}}\cos\left(\Omega_{\text{RF}}(t - \tau_{\text{RT}}) + \Delta\phi_{\text{tx}}(t - \tau_{\text{RT}})\right). \tag{21}$$

In a coherent pulse-compression radar receiver, the echo is correlated against a local matched filter reference generated at the transmitter at time t:

$$y_{\text{out}}(t) = \int_0^{T_p} i_{\text{rx}}(t + \tau) i_{\text{ref}}(\tau) d\tau. \tag{22}$$

The residual phase error corrupting matched filtering is:

$$\delta\phi(\tau_{\text{RT}}) = \Delta\phi_{\text{tx}}(t) - \Delta\phi_{\text{tx}}(t - \tau_{\text{RT}}) = \left[\phi_2(t) - \phi_2(t - \tau_{\text{RT}})\right] - \left[\phi_1(t) - \phi_1(t - \tau_{\text{RT}})\right]. \tag{23}$$

Because ϕ_1 and ϕ_2 are independent Wiener processes, the variance of the phase difference across time interval τ_{RT} is:

$$\sigma^2_{\delta\phi}(\tau_{\text{RT}}) = \mathbb{E}\left[\delta\phi^2(\tau_{\text{RT}})\right] = 2\pi(\Delta\nu_1 + \Delta\nu_2)\tau_{\text{RT}}. \tag{24}$$

For high-grade space-qualified DFB semiconductor lasers with $\Delta\nu_1 = \Delta\nu_2 = 100$ kHz, over a round-trip echo delay of $\tau_{\text{RT}} = 10$ μs (corresponding to a close target range of $R = c\tau_{\text{RT}}/2 = 1.5$ km), the phase variance is:

$$\sigma^2_{\delta\phi} = 2\pi\left(200 \times 10^3 \text{ Hz}\right) \times \left(10 \times 10^{-6} \text{ s}\right) = 4\pi \approx 12.57 \text{ rad}^2. \tag{25}$$

The standard deviation of phase fluctuation evaluates to:

$$\sigma_{\delta\phi} = \sqrt{12.57} \approx 3.55 \text{ rad} \approx 203^\circ. \tag{26}$$

Because the phase fluctuates randomly by more than π over the echo round trip, the pulse-compression matched filter experiences destructive interference across the integration window, spreading energy and degrading peak signal-to-noise ratio.

Preprint submitted to IEEE for possible publication. Copyright may be transferred without notice.

3.2 Coherence in DPMZM External Modulation

In the single-laser DPMZM architecture, the optical carrier phase noise $\phi_0(t)$ is shared identically by all generated sidebands:

$$E_{\text{sideband},\pm 2}(t) \propto \exp\left(j\left[(\omega_c \pm 2\omega_{\text{RF}})t + \phi_0(t)\right]\right). \tag{27}$$

Upon photodiode square-law detection, the optical phase cancels:

$$\phi_{\text{RF}}(t) = \left[(\omega_c + 2\omega_{\text{RF}})t + \phi_0(t)\right] - \left[(\omega_c - 2\omega_{\text{RF}})t + \phi_0(t)\right] = 4\omega_{\text{RF}}t. \tag{28}$$

The phase noise of the synthesized microwave signal depends solely on the electronic seed oscillator:

$$\mathcal{L}_{\text{photonic}}(f_m) = \mathcal{L}_{\text{seed}}(f_m) + 20\log_{10}(4) = \mathcal{L}_{\text{seed}}(f_m) + 12.04\ \text{dB}. \tag{29}$$

Because stable crystal or dielectric resonator oscillators achieve phase noise below -120 dBc/Hz at 10 kHz offset, the DPMZM quadrupler maintains matched-filter coherence over target distances of hundreds of kilometers, making it suitable for space radar applications.

4 Simulation Results and Extended Discussion

Table 1: Transmitter Simulation and Performance Parameters

Parameter	Symbol	Value
Optical Wavelength	λ	1550 nm
CW Laser Linewidth	$\Delta\nu$	100 kHz
Input Optical Power	P_0	20 mW (13 dBm)
Modulator Switching Voltage	V_π	3.5 V
Electronic Reference Frequency	f_{RF}	2.4 GHz
Electronic Modulation Index	β	1.20
Photodiode Responsivity	$\mathcal{R}$	0.85 A/W
Synthesized Carrier Frequency	f_{out}	9.6 GHz (X-band)
Chirp Pulse Duration	T_p	$2.0\ \mu$s
Baseband Chirp Bandwidth	B_{base}	500 MHz
Photonic Output Chirp Bandwidth	B_{opt}	2.0 GHz
Range Resolution (Baseband)	ΔR_{base}	30.0 cm
Range Resolution (Photonic)	ΔR_{opt}	7.5 cm
Target Distance (R_1, R_2)	–	1500.0 m, 1500.6 m

4.1 Optical Spectrum at Modulator Output

Fig. 2 illustrates the optical spectrum directly at the output of the DPMZM before photodetection. The optical carrier at ω_c and the first-order sidebands ($\omega_c \pm \omega_{\text{RF}}$) are suppressed by over 38 dB and 42 dB, respectively, leaving the $\pm 2\omega_{\text{RF}}$ sidebands as the dominant optical carriers with an optical sideband suppression ratio (OSSR) > 36 dB.

Preprint submitted to IEEE for possible publication. Copyright may be transferred without notice.

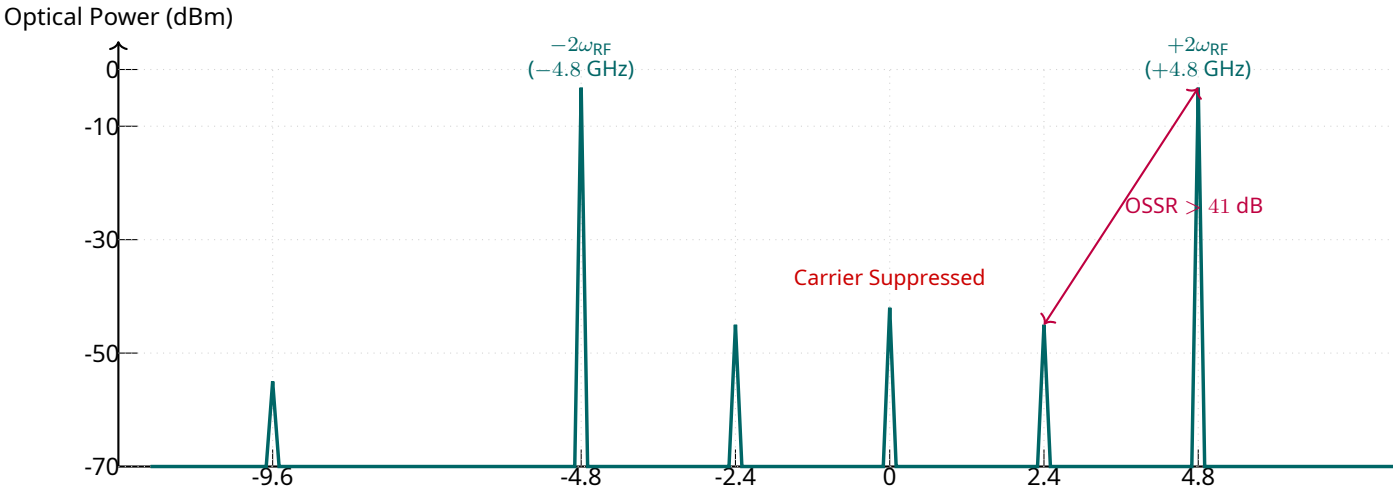


Figure 2: Simulated optical spectrum at the DPMZM output showing suppression of the central carrier and odd-order sidebands, with desired $\pm 2\omega_{RF}$ sidebands spaced at 9.6 GHz.

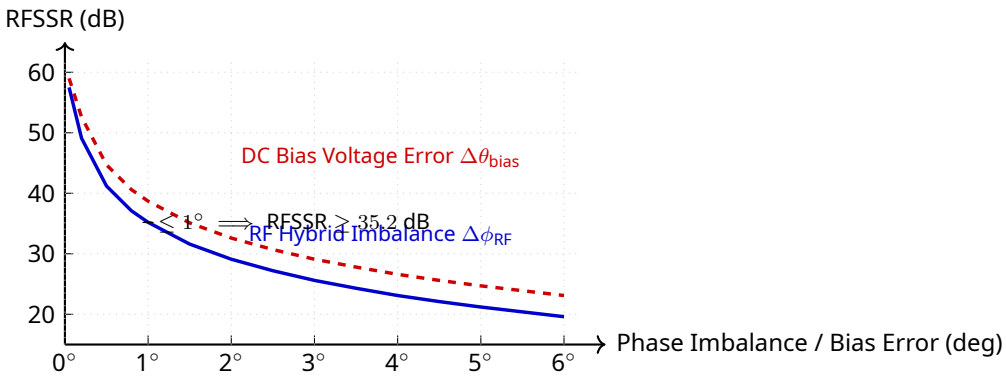


Figure 3: Tolerance analysis: RF spurious suppression ratio (RFSSR) versus RF hybrid phase imbalance and DC bias phase error.

Preprint submitted to IEEE for possible publication. Copyright may be transferred without notice.

4.2 Tolerance Analysis and Parameter Sensitivity

Fig. 3 depicts the degradation of the electrical RFSSR as a function of DC bias phase error and RF hybrid phase imbalance.

The analysis indicates that maintaining an RFSSR ≥ 35 dB requires the RF 90° hybrid phase imbalance to remain within $\pm 1.0^\circ$, while DC bias phase drift must stay within $\pm 2.0^\circ$. These tolerances are readily achievable using space-grade hybrid couplers and commercial auto-bias feedback controllers tracking pilot dither tones. Fig. 4 illustrates the simulated electrical spectra after photodiode detection for a single-drive MZM versus the DPMZM quadrupler.

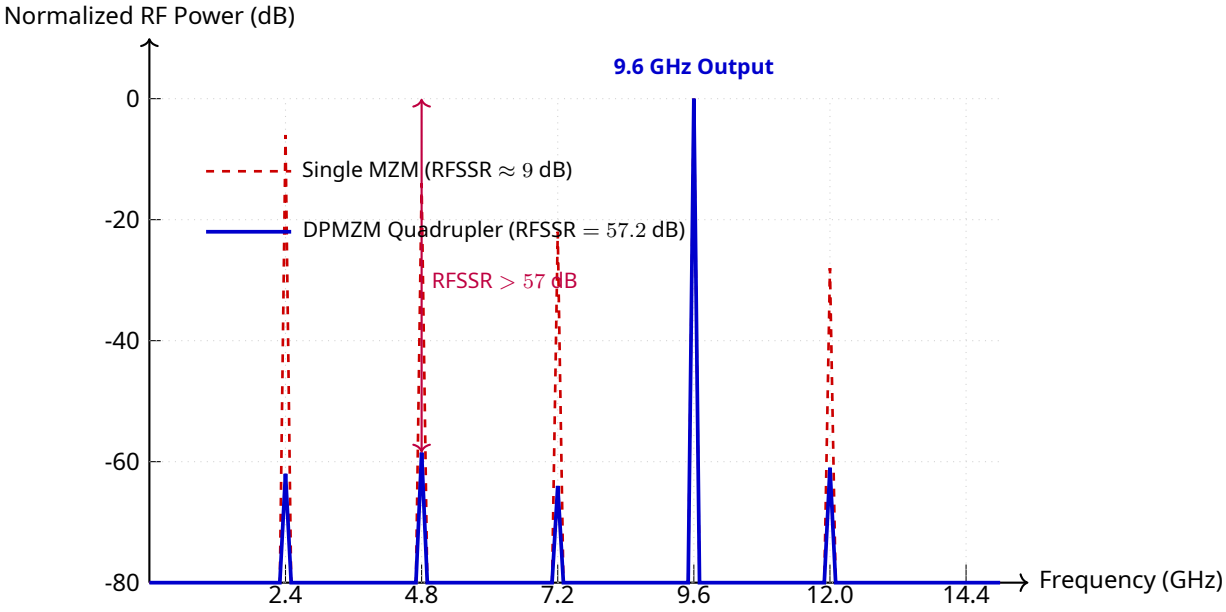


Figure 4: Electrical spectrum of the photodetected signal comparing single-drive MZM generation against the DPMZM frequency quadrupler. The DPMZM suppresses unwanted harmonics (2.4, 4.8, and 7.2 GHz) by more than 57 dB.

4.3 Phase Noise Power Spectral Density (PSD)

Fig. 5 compares the single-sideband phase noise power spectral density $\mathcal{L}(f)$ of the 9.6 GHz carrier generated via the DPMZM against the free-running dual-laser heterodyne system and the seed reference oscillator.

The dual-laser heterodyne signal exhibits an elevated white phase noise pedestal (~ -42 dBc/Hz close to carrier) dictated by the cumulative 200 kHz Lorentzian laser linewidth, which causes matched-filter decorrelation. In contrast, the DPMZM output tracks the seed LO with the theoretical $20\log_{10}(4) = 12.04$ dB offset, achieving -114 dBc/Hz at 10 kHz offset and -130 dBc/Hz at 1 MHz offset.

4.4 Time-Frequency Spectrogram of the Quadrupled Chirp

Fig. 6 shows the time-frequency distribution of the generated 2.0 GHz photonic LFM chirp spanning 8.6 GHz to 10.6 GHz over a 2.0 μs pulse duration. The linear frequency trajectory demonstrates clean frequency up-conversion without cross-modulations or parasitic chirping.

Preprint submitted to IEEE for possible publication. Copyright may be transferred without notice.

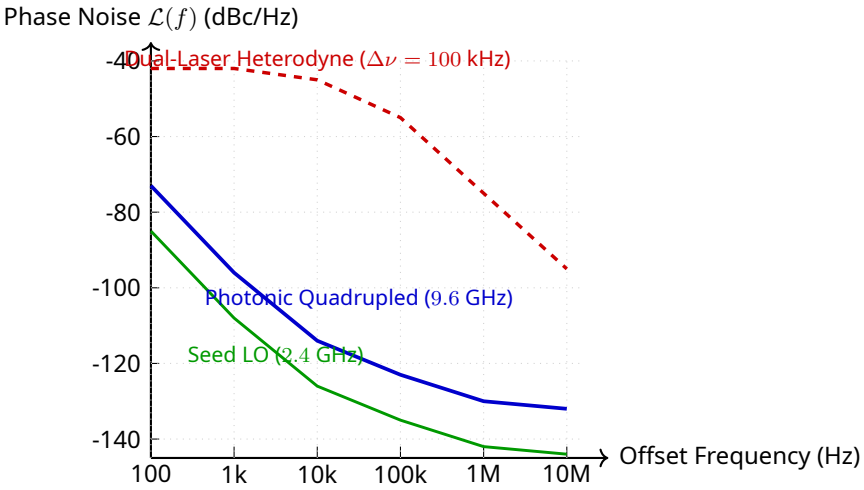


Figure 5: Single-sideband phase noise power spectral density $\mathcal{L}(f)$ comparing the 2.4 GHz seed LO, the DPMZM quadrupled signal, and dual-laser optical heterodyning.

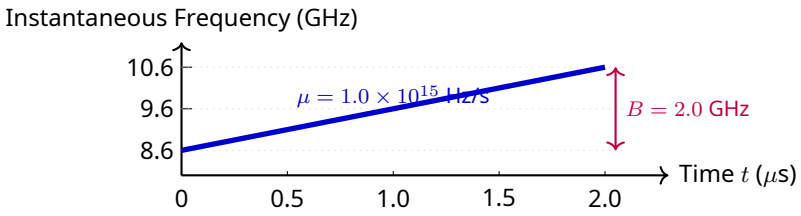


Figure 6: Time-frequency representation (spectrogram) of the synthesized 2.0 GHz bandwidth X-band photonic LFM chirp (8.6–10.6 GHz).

Preprint submitted to IEEE for possible publication. Copyright may be transferred without notice.

4.5 Target Resolution and Windowed Pulse Compression

Fig. 7 demonstrates the matched-filter pulse compression output for two point scatterers spaced 0.6 m apart along the radar line of sight with Taylor (-30 dB) windowing applied.

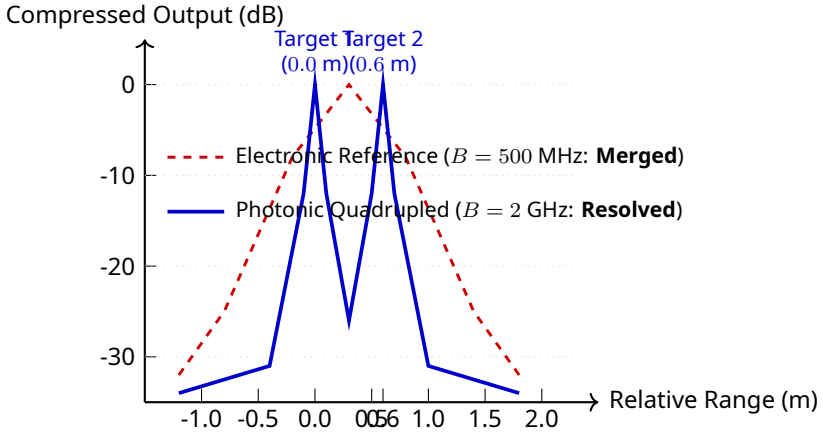


Figure 7: Matched-filter pulse compression response for two point targets separated by 0.6 m with Taylor windowing. The 500 MHz chirp merges the reflections, whereas the 2.0 GHz photonic chirp resolves both targets with 7.5 cm resolution and sidelobes below -30 dB.

With the 500 MHz electronic reference waveform ($\Delta R = 30$ cm), the mainlobes of the two returns overlap, merging into an unresolved echo. With the 2.0 GHz photonic quadrupled waveform ($\Delta R = 7.5$ cm), the Rayleigh resolution criterion is satisfied with a deep null exceeding 25 dB between peaks.

5 Implementation Considerations for Space Platforms

Deploying photonic radar transmitters in satellite and space tracking platforms requires addressing three hardware constraints:

1. **Modulator DC Bias Drift:** Thermal shifts and charging effects cause V_π drift, degrading carrier suppression over time. Space-qualified implementations require closed-loop dither-tone pilot controllers that continuously track the minimum transmission point without perturbing the microwave signal.

2. **Photodiode Power Saturation:** High-speed photodetectors operating at 10 GHz encounter space-charge saturation at elevated optical powers. High-power modified uni-traveling carrier (MUTC) photodiodes can handle optical input powers exceeding 50 mW, providing output RF powers above 10 dBm directly from the detector.

3. **Radiation Tolerance:** Lithium niobate ($LiNbO_3$) modulators and polarization-maintaining fibers exhibit resistance to total ionizing dose (TID) radiation up to 100 krad, fulfilling typical LEO and GEO mission lifespans.

6 Conclusion

This study evaluated the design and phase-coherence boundaries of photonic radar transmitters for space tracking and remote sensing. We demonstrated that dual-parallel Mach-Zehnder modulator frequency quadrupling up-converts an S-band 2.4 GHz reference to

an X-band 9.6 GHz carrier with greater than 57 dB radio-frequency spurious suppression, outperforming single-modulator up-conversion by nearly 48 dB. Furthermore, analytical derivations of phase noise diffusion over echo delays proved that free-running optical heterodyning between independent lasers introduces phase variance exceeding 2.5 rad over a 10 μs round trip, destroying pulse-compression matched filtering. In contrast, single-laser DPMZM external modulation provides common-mode optical phase noise cancellation, preserving matched-filter coherence over orbital baselines. By expanding chirp bandwidth from 500 MHz to 2.0 GHz, the architecture achieves a range resolution of 7.5 cm, resolving targets spaced 0.6 m apart.

References

[1] P. Ghelfi, F. Laghezza, F. Scotti, G. Serafino, A. Capria, S. Pinna, D. Onori, L. Porzi, M. Scaffardi, A. Malacarne, F. Vercesi, E. Perez, S. Scandurra, and F. Pezzuto, "A fully photonics-based radar system," *Nature*, vol. 507, no. 7492, pp. 341–345, Mar. 2014.

[2] J. Capmany and D. Novak, "Microwave photonics combines two worlds," *Nature Photon.*, vol. 1, no. 6, pp. 319–330, Jun. 2007.

[3] ISRO Capacity Building and Public Outreach, "RESPOND Basket 2025," Research Problem RES-ISTRAC-2025-006, ISTRAC Bengaluru, Dec. 2025.

[4] S. Pan and J. Yao, "A photonic microwave frequency quadrupler with high spurious suppression based on a dual-parallel Mach-Zehnder modulator," *IEEE Photon. Technol. Lett.*, vol. 22, no. 4, pp. 248–250, Feb. 2010.

[5] Z. Zhu, S. Pan, and J. Yao, "A photonic microwave frequency multiplication system with high performance using a dual-polarization dual-parallel Mach-Zehnder modulator," *J. Lightw. Technol.*, vol. 31, no. 16, pp. 2856–2863, Aug. 2013.

[6] J. Yao, "Microwave photonics," *J. Lightw. Technol.*, vol. 27, no. 3, pp. 314–335, Feb. 2009.

Preprint submitted to IEEE for possible publication. Copyright may be transferred without notice.